Title

Hydrolysis of Small Oxo/Hydroxo Molecules Containing High Oxidation State Actinides (Th, Pa, U, Np, Pu): A Computational Study

Journal

The Journal of Physical Chemistry A, 125(28)

ISSN

1089-5639

Authors

Lontchi, Eddy M

Vasiliu, Monica

Tatina, Lauren M

et al.

Publication Date

2021-07-22

DOI

10.1021/acs.jpca.1c04048

Peer reviewed

Hydrolysis of Small Oxo/Hydroxo Molecules Containing High Oxidation State Actinides (Th, Pa, U, Np, Pu): A Computational Study

Eddy M. Lontchi,[1] Monica Vasiliu,[1] Lauren M. Tatina,[1] Alyssa C. Caccamo,[1] Amber N. Gomez,[1] John K. Gibson,[2] and David A. Dixon[1,*,2]

[1] Department of Chemistry and Biochemistry, The University of Alabama, Shelby Hall, Tuscaloosa AL 35487-0336

[2] Chemical Sciences Division. Lawrence Berkeley National Laboratory, Berkeley, CA 94720

Abstract

The energetics of hydrolysis reactions for high oxidation states oxo/hydroxo monomeric actinide species ($Th^{IV}O_2$, $Pa^{IV}O_2$, $U^{IV}O_2$, $Pa^{V}O_2(OH)$, $U^{V}O_2(OH)$, $U^{VI}O_3$, $Np^{VI}O_3$, $Np^{VII}O_3(OH)$, and $Pu^{VII}O_3(OH)$) were calculated at the CCSD(T) level. The first step is formation of a Lewis acid/base adduct with H_2O (hydration), followed by proton transfer to form a dihydroxide molecule (hydrolysis); this process is repeated until all oxo groups are hydrolyzed. The physisorption (hydration) for each H_2O addition was predicted to be exothermic, *ca.* -20 kcal/mol. The hydrolysis products are preferred energetically over the hydration products for the +IV and +V oxidation states. The compounds with An^{VI} are a turning point in terms of favoring hydration over hydrolysis. For $An^{VII}O_3(OH)$, hydration products are preferred and only 2 waters can bind; the complete hydrolysis process is now endothermic and the oxidation state for the An in $An(OH)_7$ is +VI with two OH groups each having one-half an electron. The NBO charges and the reaction energies provide insights into the nature of the hydrolysis/hydration processes. The actinide charges and bond ionicity generally decrease across the Period. Ionic character

[2] Email: dadixon@ua.edu

decreases as the oxidation state and coordination number increase so that covalency increases moving to the right in the actinide Period.

Introduction

Hydrolysis reactions are important in transformations of metal oxides into hydroxides. We have previously explored the hydrolysis mechanism of small $(MO_2)_n$ (M = Ti, Zr, Hf, n =1-4) nanoclusters, by adding up to two H_2O molecules, using DFT and CCSD(T).[1,2] For hydrolysis of $(MO_2)_n$ (M = Ti, Zr, Hf, n = 1-4), it was found that the physisorption energies depend on the cluster size and the adsorption site. The initial H_2O physisorption energies for the ground singlet state of MO_2 were predicted to be -10 to -35 kcal/mol. The energetics for the first hydrolysis reaction on the ground singlet state of MO_2 nanoclusters were predicted to be -20 to -80 kcal/mol. In these transition metal oxide clusters, the calculations showed that H_2O readily reacts with an M=O group to form the hydroxides.

Actinide (An) elements play a major role as materials in nuclear energy, and their generated waste can introduce storage issues leading to environmental concerns and health related issues in the event of exposure.[3,4] Actinide hydrolysis reactions can impact environmental transport, nuclear fuel processing, and waste treatment and disposition. The interactions of actinyls with water have been studied experimentally[5,6,7,8,9,10,11,12] and computationally.[13,14,15,16,17,18,19,20,21] We used the high level Feller-Peterson-Dixon (FPD) approach[22,23,24,25] (coupled cluster theory with single and double excitations and an approximate triples correction (CCSD(T)) extrapolated to the complete basis set limit plus additional corrections) to predict potential energy surfaces for the oxo-exchange via hydrolysis of $AnO_2^{0/+/2+}$ for An = $Th^{IV}O_2^0$, $Pa^{V}O_2^+$, $U^{V}O_2^+$ and $U^{VI}O_2^{2+}$ with results in agreement with the available experiments.[26] Neutral actinide oxo/hydroxo compounds have been studied as well.[27,28] McKee and Gorden further expanded on Th hydrolysis, and explored the hydrolysis mechanisms of $ThO_2(H_2O)_n$, n = 1, 2, 4, at the CCSD(T) and DFT/M06 levels of theory.[29] Tsushima predicted

that two $Th(OH)_4(OH_2)_2^0$ molecules can be connected via hydrogen bonds to form the OH-bridged dimer complex $Th_2(OH)_8^0$.[30] As another example, Gibson and co-workers studied gas-phase reactions of actinyl-oxolate complexes with H_2O and O_2 in a quadrupole ion trap.[31] Their results showed that water addition to UO_4^- was spontaneous, forming the hydrate, $UO_4(H_2O)^-$, and the hydroxide, $UO_3(OH)_2^-$.

The overall objective of the present work is to expand our work on actinide oxide hydrolysis to study the hydrolysis of the neutral early actinide oxides and mixed actinide oxides/ hydroxides monomers in their highest oxidation states, including ThO_2, $PaO_2(OH)$, AnO_3 (An = U, Np), $AnO_3(OH)$ (An = Np, Pu). We did not pursue the +VIII oxidation state represented by PuO_4 due to the complexity of its structure;[32] our preliminary studies showed that the optimized C_{2v}, $^5Pu^{V}O_2(O_2^-)$ structure is the lowest energy isomer and is more stable than the isomeric $^1Pu^{VIII}O_4$, D_{4h} structure by ~7 kcal/mol at the CCSD(T)/aD-DK level. Enough H_2O molecules are added to convert each oxo (O^{2-}) ligand into two hydroxy (OH^-) groups. A goal is to predict the reaction energetics and the stability of the hydroxylated products relative to oxo or oxo/hydroxo reactants and intermediates with H_2O bonded in a Lewis acid/base interaction. The initial step is formation of a Lewis acid/base adduct, followed by a proton transfer converting an O^{2-} to a di-hydroxide; this process is repeated until all oxo groups are hydrolyzed. Physisorption energies, hydrolysis energies, and reaction barriers have been calculated to generate reaction coordinates. The DFT reaction coordinates for these monomers were benchmarked by comparing with those calculated at the CCSD(T) level.

Computational Methods

Geometries were optimized at the density functional theory (DFT)[33] level with the B3LYP exchange-correlation functional,[34,35] which we have previously shown[26] to give

reasonable structures for such species. The aug-cc-pVDZ basis sets[36,37] for O and H, the cc-pVDZ-PP basis sets with effective core potentials were used for An = Th, Pa, and U.[26,38,39,40] and the Stuttgart small core relativistic effective core potential (60ECP) with the accompanying segmented basis set were used for Np and Pu.[41,42,43] We denote these basis sets as aD-PP. Vibrational frequencies were calculated to show that the structures were minima or transition states. The DFT calculations were carried out with the Gaussian16 program system.[44]

To improve the energetics, additional single-point energy calculations using the DFT optimized geometries, were performed at the coupled cluster CCSD(T) level of theory[45,46,47,48] using the 3rd-order Douglas-Kroll-Hess Hamiltonian[49,50,51] with the aug-cc-pV*n*Z-DK for H,[52] aug-cc-pV*n*Z-DK for O,[36,53] cc-pV*n*Z-DK3 for An = Th-Pu[26,38,54] for n = D for all species, and additional n = T basis sets for the singlet ground state species (Supporting Information). We denote these basis sets as a*n*-DK for n = D and T. All CCSD(T) calculations were performed with the MOLPRO 2018 program.[55,56]

For many of the open shell molecules, especially the initial species to be hydrolyzed, where it was not possible to readily assign the correct starting occupations for the different spin-symmetry states based on the DFT calculations, we performed CASSCF[57,58] calculations to obtain the correct starting orbital occupancies for the restricted open shell Hartree-Fock (ROHF) and CCSD(T) calculations. The open-shell CCSD(T) calculations were done with the R/UCCSD(T) approach where an ROHF calculation was initially performed and the spin constraint was then relaxed in the coupled cluster calculation.[59,60,61,62]

The calculated reaction energies do not take into account any corrections due to spin-orbit coupling. $Th^{IV}O_2$, $Pa^{V}O_2(OH)$, $U^{VI}O_3$, and $Np^{VII}O_3(OH)$ are closed shell molecules and there are no spin-orbit corrections to first order. The remaining monomers, $Pa^{IV}O_2$, $U^{IV}O_2$, $U^{V}O_2(OH)$,

$Np^{VI}O_3$, and $Pu^{VII}O_3(OH)$, are open shell structures so there can be first-order spin-orbit effects. However, we do not expect the relative spin-orbit corrections on the hydrolysis reaction coordinates to be large as differences in the spin-orbit corrections should be small due to cancellation of errors. The errors in the relative spin-orbit corrections between different species on the reaction coordinates should be comparable in magnitude to the errors due to the use of the aD-DK basis sets.

The Natural Population Analysis (NPA) results based on the Natural Bond Orbitals (NBOs)[63,64] using NBO7[65,66] are calculated using MOLPRO 2018. The calculations were done on our local UA Opteron- and Xeon-based Linux clusters and at the Molecular Sciences Computing Facility in the William R. Wiley Environmental Molecular Sciences Laboratory at the Pacific Northwest National Laboratory.

Results and Discussion

Geometries The optimized geometries at the DFT/B3LYP level are reported in Table 1 for the initial monomeric, to hydrolyze structures. First, we consider the +IV oxidation state. The ground state structure for ThO_2 with Th atom in +IV formal oxidation state is bent with C_{2v} symmetry and is a singlet. Thus, ThO_2 is similar to Group IV transitional metals oxides, MO_2. The computational and experimental ThO_2 vibrational spectra and geometry have been previously reported.[67,68] The ground states for $^2PaO_2$ and $^3UO_2$ are linear with Pa and U in the formal +IV oxidation state with $7s^1$ and $7s^15f^1$ electron configurations, respectively. The ground states of $^3UO_2$ has been previously assigned.[69] CASSCF calculations were used to determine the ground state for the CCSD(T) calculations of $^2PaO_2$ and the excited d^1 and f^1 states are ~22 and

49 kcal/mol, respectively, higher in energy at CCSD(T)/aD-DK level. The Pa-O and U-O bond distances are ~0.09 Å and 0.11 Å, respectively, shorter than Th-O in ThO_2.

For the +V oxidation state, $Pa^{V}O_2(OH)$ is planar with 2 axial Pa-O actinyl bonds that are almost identical in bond length, and a longer Pa-O(H) equatorial bond. $PaO_2(OH)$ has a similar geometry to that of $U^{VI}O_3$ with a Pa-OH equatorial instead of a U-O equatorial group. $^2UO_2(OH)$, with U in +V formal oxidation state and a $5f^1$ electron occupancy, has a similar structure to $PaO_2(OH)$. The actinyl U-O and the axial U-O(H) bonds are ~0.02 Å and ~0.01 Å, respectively, shorter than the corresponding bonds in $PaO_2(OH)$.

For the +VI oxidation state, UO_3 is predicted to have two axial oxygens forming a uranyl dication moiety, and the third oxygen (formally O^{2-}) in an equatorial position with a longer U-O bond distance.[69,70] The U is in the formal +VI oxidation state with no active valence electrons. The structure of UO_3 differs from that of transition metal oxides such as WO_3 and MoO_3 which have three equivalent M-O bonds in C_{3v} symmetry for the +VI oxidation state of metal.[71,] Similar to UO_3, NpO_3 has C_{2v} symmetry with both axial and equatorial Np-O bond distances shorter by about 0.03 Å as compared to those in UO_3. The ground state for NpO_3 is $^2A_2$ with $5f^1$ electron configuration.[72] The $\angle O_{ax}$-An-O_{ax} in NpO_3 is 9 degrees larger than in UO_3.

Table 1. Optimized geometry parameters (bond distances in angstroms (Å) and bond angles in degrees (°)) at B3LYP level for all monomeric to hydrolyze structures.

Molecule	**Sym**	**State**	**An-O_{ax}**	**An-O_{eq}/ An-O(H)**	**$\angle O_{ax}$-An-O_{ax}/ $\angle O_{ax}$-An-O(H)$_{ax}$**	**$\angle O_{eq}$-An-O_{ax}/ $\angle$O-An-O(H)**	**An-OH_2[b]**	**An-OH_2[c]**
$^1ThO_2$	C_{2v}	$^1A_1$	1.910		121.1		2.637	2.667
$^2PaO_2$	$D_{\infty h}$	$^2\Sigma_g$	1.816		180.0		2.512	2.551
$^3UO_2$	$D_{\infty h}$	$^3\Phi_g$	1.802		180.0		2.531	2.537
$^1PaO_2(OH)$	C_s	$^1A'$	1.840,1.844[a]	/2.159	161.1	100.1,98.8[a]	2.552	2.589
$^2UO_2(OH)$	C_s	$^2A'$	1.820,1.821[a]	/2.147	167.7	97.7,94.6[a]	2.543	2.583
$^1UO_3$	C_{2v}	$^1A_1$	1.813(x2)	1.856	157.3	101.3	2.544	2.587
$^2NpO_3$	C_{2v}	$^2A_2$	1.778 (x2)	1.829	166.1	97.0	2.522	2.596
$^1NpO_3(OH)$	C_s	$^1A'$	1.769, 1.775[a]	1.808/2.086	172.3/179.0	93.6,94.2/ 85.5,86.8[a]	2.534	2.571[d]
$^2PuO_3(OH)$	C_s	$^2A''$	1.751,1.759[a]	1.798/2.072	173.7/178.9	92.8,93.5/ 86.1,87.6[a]	2.519	2.558[d]

[a] towards H(O); [b] An-OH_2 for the first water adduct. [c] An-OH_2 for the 2 water physiosorbed species. [d] average

Heptavalent $Np^{VII}O_3(OH)$ also has a planar structure. The Np-O axial bonds are not identical, as found for $PaO_2(OH)$, with the Np-O bond closest to the equatorial H-(O-Np) slightly longer by less than 0.01 Å. The Np-O(H) bond is 0.07 Å longer than the Pa-O(H) bond in $PaO_2(OH)$. Heptavalent $PuO_3(OH)$ has a $^2A''$ ground state structure ($5f^1$ electron configuration), which is very similar to the corresponding $NpO_3(OH)$ structure. Again, the axial Pu-O bonds are not the same length and the axial Pu-O are about 0.02 Å shorter than the axial Np-O bonds in $NpO_3(OH)$. The equatorial Pu-O and Pu-O(H) bonds are about 0.01 Å shorter than the corresponding bonds in $NpO_3(OH)$. In terms of bond angles, there is no significant change observed in heptavalent $AnO_3(OH)$ structures for An = Pu and Np. The $\angle O_{ax}$-An-O_{ax} angle in $AnO_3(OH)$ structures is more than 10 degrees larger than observed in pentavalent $PaO_2(OH)$.

Hydrolysis Reactions. *Hydrolysis of An(IV)* The results for $Th^{IV}O_2$ are shown in Table 2 at different levels of theory (new and previously reported)[26,73] and in Figure 1 at the CCSD(T)/aD-DK level. The current CCSD(T)-DK results are consistent with our prior work[26] on the hydrolysis of ThO_2 and that of others.[29] The initial step is formation of a Lewis acid/base adduct between ThO_2 and H_2O. Proton transfer to a Th=O has a very low barrier and leads to formation of the di-hydroxide in a very exothermic process. The addition of a second H_2O leads to a Lewis acid/base complex with about the same binding energy as for addition of the first H_2O. The barrier to form the tetra-hydroxide is again very low and formation of $Th(OH)_4$ is an overall exothermic process leading to complete hydrolysis of ThO_2. Overall, the basis set size or the way that scalar relativistic effects are incorporated does not impact the energetics. The B3LYP values are all less exothermic than the CCSD(T) values and the differences increase with adding the second H_2O.

Table 2. Reaction (ThO_2 + H_2O) energies (ΔH_{298K}) in kcal/mol

Product	**B3LYP**[a]	**CCSD(T)-DK**[b]		**CCSD(T)-PP**[c]		**CCSD(T)/CBS**[d]
		n = D	n = T	n = T	CBS	
$(H_2O)ThO_2$	-18.4	-21.5	-21.1	-21.1	-20.7	-20.3
$(H_2O)ThO_2$ (TS1)	-18.1	-20.2	-19.7	-19.9	-19.3	-18.5
$ThO(OH)_2$	-57.2	-60.0	-58.8	-59.3	-58.9	-58.7
$(H_2O)ThO(OH)_2$	-75.0	-81.4	-79.6	-80.1	-79.3	
$(H_2O)ThO(OH)_2$(TS2)	-74.8	-80.2	-78.5	-79.3	-78.3	
$Th(OH)_4$	-116.8	-123.6	-121.2	-122.6	-121.9	

[a] aug-cc-pVDZ(H,O)/cc-pVDZ -PP(Th). [b] (aug-)cc-pVnZ-DK3. c (aug-)cc-pVnZ-PP from Ref. 73. [d]CCSD(T)/CBS(awCVnZ)/PW91+SO +ECP correction from Ref. 26.

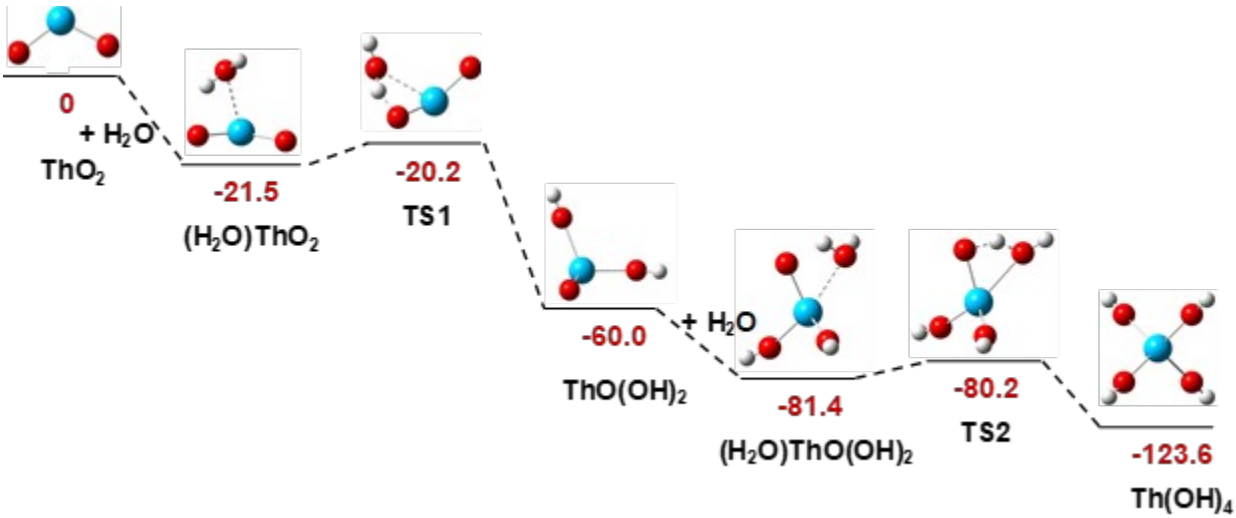

Figure 1. Reaction coordinate energies (ΔH_{298K}) in kcal/mol at CCSD(T)/aD-DK for ThO_2 hydrolysis. Thorium in blue, Oxygen in red and Hydrogen white.

The results for the hydrolysis of PaO_2 and UO_2 are reported in Figure 2. The hydrolysis energetics are similar for PaO_2 and UO_2 and are less exothermic than ThO_2 hydrolysis. The initial

step with formation of a Lewis acid/base adduct is less exothermic by 4 to 5 kcal/mol for PaO_2 and UO_2 than for ThO_2. Proton transfer to a Pa=O has a barrier of ~16 kcal/mol, which is much higher than that predicted for ThO_2, but is still below the reactant asymptote. Proton transfer to a U=O is predicted to have an even higher barrier of ~22 kcal/mol and the barrier is now above the reactant asymptote. The formation of the di-hydroxide for both Pa and U are still very exothermic processes, although the exothermicity is about one-half that for ThO_2. The chemisorbed, di-hydroxide species are non-planar structure for all 3 actinides.

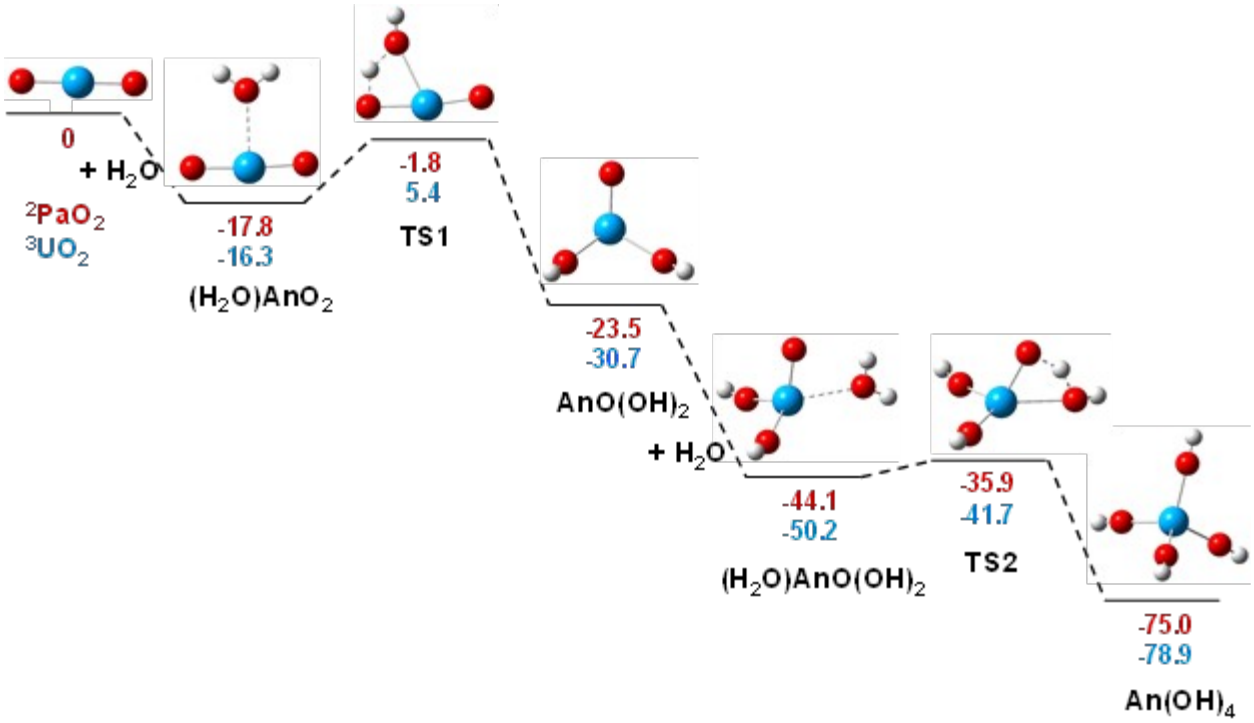

Figure 2. Reaction coordinate energies (ΔH_{298K}) in kcal/mol at CCSD(T)/aD-DK for $^2PaO_2$ in red and $^3UO_2$ hydrolysis in blue. Actinide in blue, Oxygen in red and Hydrogen white.

The addition of a second H_2O leads to a Lewis acid/base complex that is comparable for all three actinides and the binding energy is slightly more favorable than the first H_2O binding for Pa and U. The barrier to form the tetra-hydroxides for Pa and U are higher (~ 8 kcal/mol for both

Pa and U) than that calculated for Th, although lower than the first water addition barrier. The formation of $Pa(OH)_4$ and $U(OH)_4$ are overall exothermic process and $U(OH)_4$ is more exothermic by 4 kcal/mol than $Pa(OH)_4$, but overall both reactions are much less exothermic than for ThO_2.

Hydrolysis of An(V) The results for hydrolysis of $Pa^{V}O_2(OH)$ are shown in Figure 3 at the CCSD(T)/aD-DK level and in the Supporting Information at DFT/B3LYP and CCSD(T)/aT-DK levels. The addition of the first H_2O to form the Lewis acid/base adduct has about the same exothermicity as for adding H_2O to ThO_2. The barrier for proton transfer to form $PaO(OH)_3$ is significantly larger than for ThO_2 but it is still below the reactant asymptote. The addition of the second H_2O is about 6 kcal/mol less exothermic than for the first step. The barrier for proton transfer is about 13 kcal/mol, about the same as the first proton transfer barrier. The exothermicity of this step is only about 10 kcal/mol. The overall exothermicity of the reaction is about 55% that for ThO_2. There are modest differences between the B3LYP and CCSD(T) values.

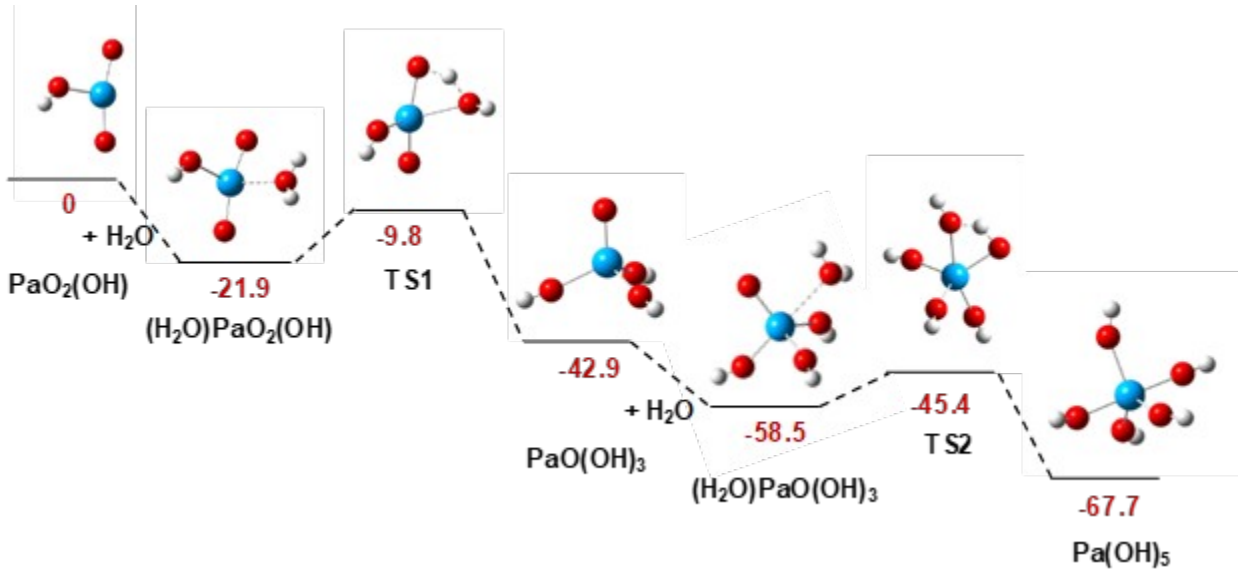

Figure 3. Reaction coordinate energies (ΔH_{298K}) in kcal/mol at CCSD(T)/aD-DK for $PaO_2(OH)$ hydrolysis. Protactinium in blue, Oxygen in red and Hydrogen white.

The results for hydrolysis of $U^{V}O_2(OH)$ are shown in Figure 4. The addition of the first H_2O to form the Lewis acid/base is an exothermic process, *ca.* -3 kcal/mol more exothermic than for the corresponding Pa structure. Formation of $(H_2O)UO_2(OH)$ is the most exothermic first water addition complex formed in the current study. The barrier for proton transfer to form $UO(OH)_3$ is ~15 kcal/mol and is below the reactant asymptote. The chemisorbed product of the first water addition, $UO(OH)_3$ is a ~9 kcal/mol less stable than its corresponding physiosorbed product, $(H_2O)UO_2(OH)$. This is different than what was calculated for $Pa^{V}O_2(OH)$. Moreover $UO(OH)_3$ and $PaO(OH)_3$ are calculated to have different geometries. $PaO(OH)_3$ optimizes to a C_{3v}-like structure whereas the lowest energy $UO(OH)_3$ is a C_{2v}-like structure with 2 equatorial OHs and an O and an OH in axial positions with a O-U-O(H) angle of 147.8º. The $UO(OH)_3$ C_{3v} symmetry structure is a minima as well and is less than 1 kcal/mol higher in energy. The addition of the second H_2O to $UO(OH)_3$ is more exothermic than the first water addition by ~6 kcal/mol. The barrier for proton transfer is about 12 kcal/mol, 3 kcal/mol less than the first proton transfer barrier. The exothermicity of this step to form the chemisorbed product, $U(OH)_5$, is only about 12 kcal/mol. The product, $U(OH)_5$ is a C_{4v}-like structure which differs from the corresponding $Pa(OH)_5$, which is a D_{3h}-like structure, with 2 axial and 3 equatorial Pa-O(H) bonds.

Hydrolysis of An(VI) The results for hydrolysis of $U^{VI}O_3$ are shown in Figure 5 at the CCSD(T)/aD-DK level and in the Supporting Information at the DFT/B3LYP and CCSD(T)/aT-DK levels. The initial Lewis acid/base adduct binding energy is essentially the same as those for ThO_2 and PaO_2OH. The initial proton transfer barrier is slightly smaller than in PaO_2OH. The

binding energy for the second H_2O is larger than for $PaO(OH)_3$ but smaller than for $ThO(OH)_2$. However, the transition state for the transfer of the proton in this step to form $UO(OH)_4$ is much higher in energy, ~ 26 kcal/mol, and $UO(OH)_4$ is less stable than $(H_2O)UO_2(OH)_2$ by 13 kcal/mol. Addition of a third H_2O leads to a complex $(H_2O)UO(OH)_4$ that is slightly more stable by 4 kcal/mol than $(H_2O)UO_2(OH)_2$. A proton transfer transition state that is ~ 27 kcal/mol separates $(H_2O)UO(OH)_4$ from $U(OH)_6$ and $U(OH)_6$ is less stable than $(H_2O)UO(OH)_4$ by 11 kcal/mol. Depending on the conditions, the sinks for hydrolysis of UO_3 are the $(H_2O)UO_2(OH)_2$ and $(H_2O)UO(OH)_4$ complexes, in contrast to hydrolysis of ThO_2 and PaO_2OH where the sinks are the fully hydroxylated $Th(OH)_4$ and $Pa(OH)_5$ species, respectively.

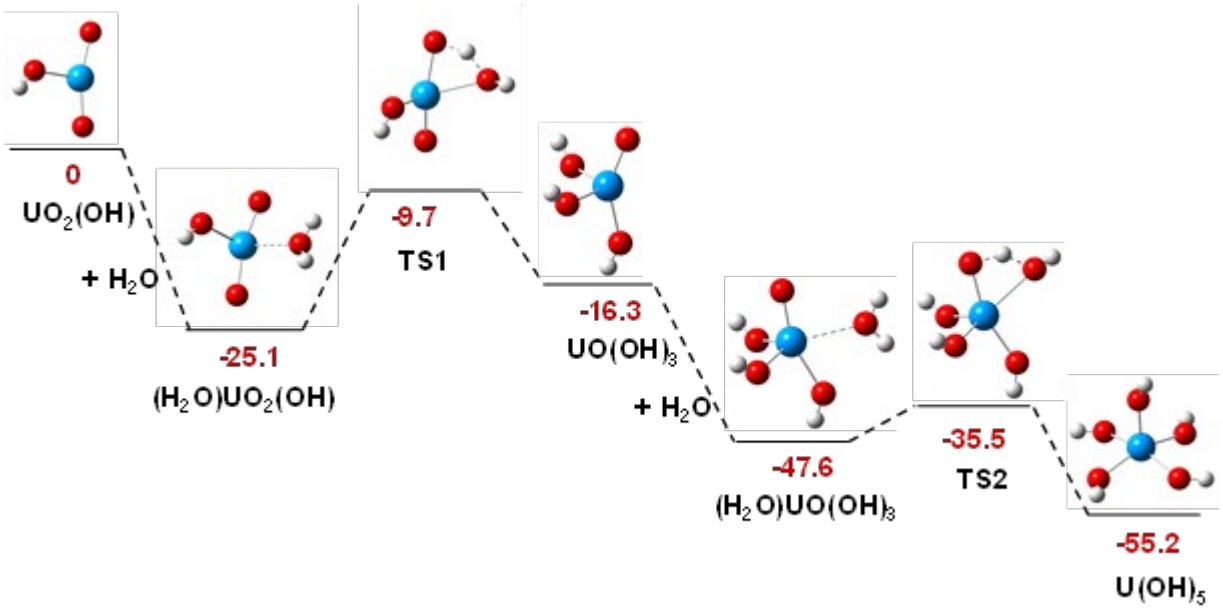

Figure 4. Reaction coordinate energies (ΔH_{298K}) in kcal/mol at CCSD(T)/aD-DK for $^2UO_2(OH)$ hydrolysis. Uranium in blue, Oxygen in red and Hydrogen white.

The hydrolysis results for $^2Np^{VI}O_3$ are shown in Figure 6 at the CCSD(T)/aD-DK level with additional energetics at different computational levels in the Supporting Information. The

energetics of $^{2}NpO_3$ hydrolysis are comparable and follow the same trends to what was calculated for the corresponding UO_3 hydrolysis. Overall, $^{2}NpO_3$ hydrolysis is up to 8 kcal/mol less exothermic than UO_3 hydrolysis with larger energy differences predicted as more water molecules

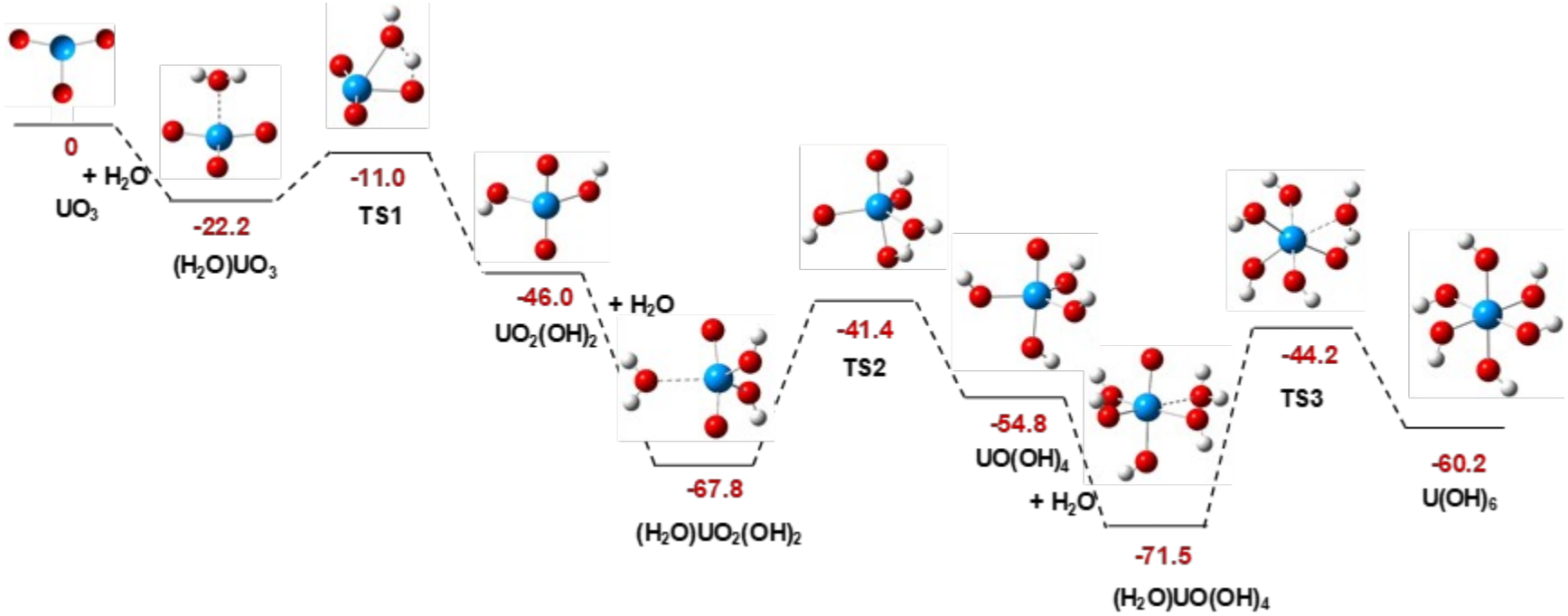

Figure 5. Reaction coordinate energies (ΔH_{298K}) in kcal/mol at CCSD(T)/aD-DK for UO_3 hydrolysis. Uranium in blue, Oxygen in red and Hydrogen white.

are added. Again, the initial chemisorbed water adduct binding energy is essentially the same as those for ThO_2, PaO_2OH and UO_3. The first chemisorption product, $AnO_2(OH)_2$ optimizes to a structure with C_2 symmetry for An = U with 2 axial U-OH's with (H)O-U-O(H) angle of 112º and O-U-O angle of 169 º and to a C_{2h} symmetry structure for An = Np. The An=O bonds are ~ 0.03 Å shorter for $NpO_2(OH)_2$ than the corresponding U species. Similar changes were predicted for the initial AnO_3 species. The An-OH bond distances in $AnO_2(OH)_2$ do not significant change for U to Np. As calculated for UO_3, the $(H_2O)NpO(OH)_4$ complex is more favorable than the fully hydroxylated species, $Np(OH)_6$.

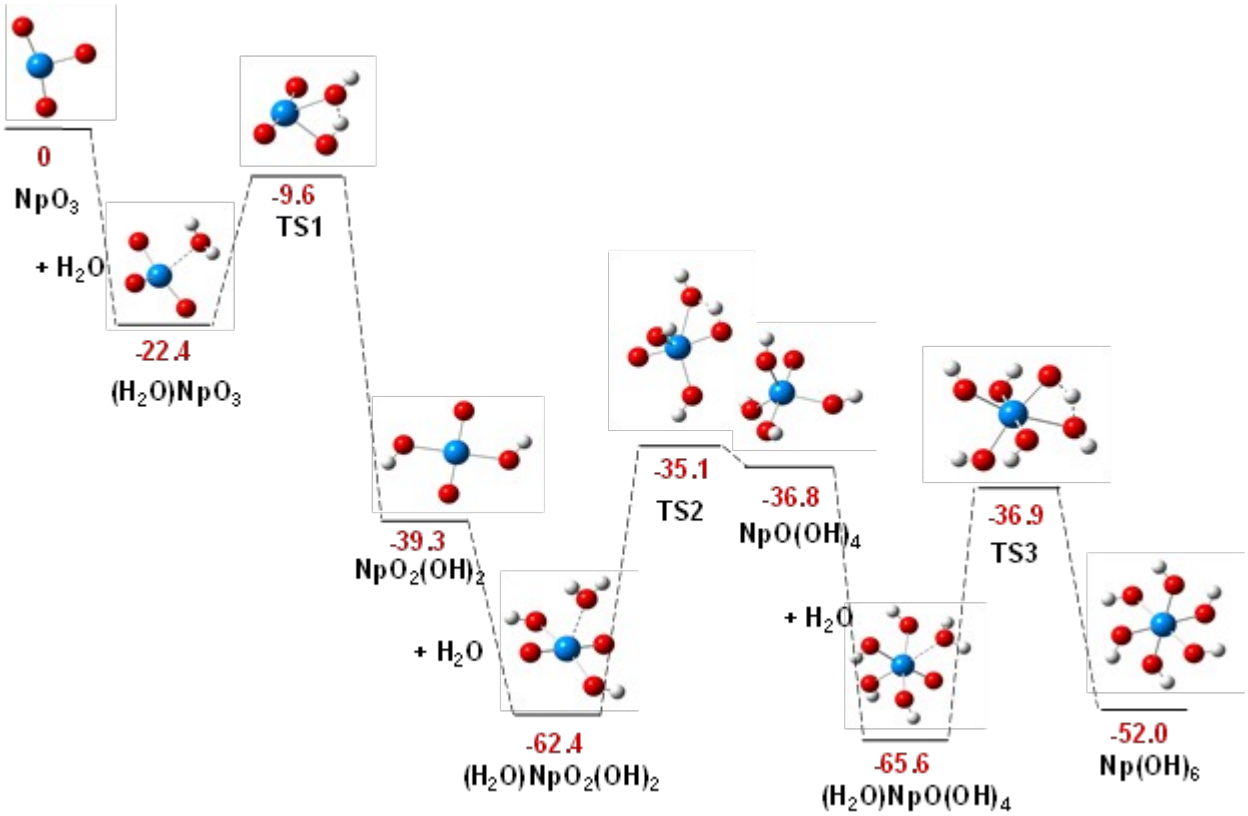

Figure 6. Reaction coordinate energies (ΔH_{298K}) in kcal/mol at CCSD(T)/aD-DK for $^2NpO_3$ hydrolysis. Neptunium in blue, Oxygen in red and Hydrogen white.

Hydrolysis of An(VII) The reaction coordinate for the hydrolysis of $Np^{VII}O_3(OH)$ at the CCSD(T)/aD-DK level is shown in Figure 7. A complication arises in the prediction of the reaction coordinate for these systems as there could be a change in the electronic structure of a complex from the +VII to the +VI oxidation state of Np or Pu, as seven OH groups may not be able to support the +VII oxidation state. The lowest energy structures for $Np(OH)_7$ and $Pu(OH)_7$ have a spin split between two of the OH groups so that the An is in the +VI oxidation state. Thus, the Np in $Np(OH)_7$ has a single unpaired electron on it and the other electron is split between two OH groups, so that the ground state is a triplet. The singlet-triplet splittings for the $Np^{VII}O_3(OH)$ hydrolysis reaction coordinate at the DFT level are given in the Supporting Information and only $Np(OH)_7$ has a triplet ground state. For $Pu(OH)_7$, the Pu is in the +VI oxidation state with two unpaired 5f electrons coupling to an electron split between two OH groups which gives a quartet ground state for $Pu(OH)_7$. The doublet-quartet splittings for the $Pu^{VII}O_3(OH)$ hydrolysis reaction coordinate are also given in the Supporting Information and, in general, the splittings decrease in size as H_2O molecules are added and O atoms are converted to OH groups. For the Pu reaction coordinate, the first transition state is also a quartet ground state with 2 unpaired spins on Pu and one spin on one OH group with a small doublet-quartet splitting.

The hydrolysis steps of the high +VII formal oxidation state Np, $NpO_3(OH)$, is calculated to be not as favorable as shown in the previously high oxidation state actinide species from Th-U. The initial water adduct is an exothermic process with energetics comparable to the initial Lewis acid-base adducts shown above for the early actinides. The barrier for proton transfer from the adduct to the first di-hydroxide intermediate has increased to 23 kcal/mol. The first water adduct and the dihydroxyl complex, $NpO_2(OH)_3$, are essentially isoenergetic. The physisorption binding energy for the second H_2O is an exothermic process and represents the lowest energy

point of the energy surface. The barrier for proton transfer to form $NpO(OH)_5$ is about 41 kcal/mol. $NpO(OH)_5$ is 30 kcal/mol less stable than the initial di-hydroxide intermediate, $NpO_2(OH)_3$. Formation of $Np(OH)_7$ is not an energetically favorable process and no water adduct or a corresponding transition state could be optimized leading to $Np(OH)_7$ from the $NpO(OH)_5$ intermediate.

The reaction coordinate for hydrolysis of $^2PuO_3(OH)$ at the CCSD(T)/aD-DK level is shown in Figure 7 as well. The hydrolysis reaction of $^2PuO_3(OH)$ follows the same trends as predicted for $NpO_3(OH)$ hydrolysis. The first barrier to transfer the proton to form $PuO_2(OH)_3$ is 2 kcal/mol lower than what was calculated for the corresponding Np structure and this transition state is a quartet. The first di-hydroxy intermediate, $PuO_2(OH)_3$, is 8 kcal/mol less stable than the initial water adduct, whereas for the corresponding Np compound, this di-hydroxy intermediate was isoenergetic with the formation of the first water adduct. The formation of the second water Lewis acid-base adduct is favorable, 5 kcal/mol less exothermic than for the corresponding Np complex. $PuO(OH)_5$ is 28 kcal/mol less stable than the initial di-hydroxide intermediate, $PuO_2(OH)_3$, and as predicted for Np, the formation of $Pu(OH)_7$ is not an energetically favorable process. Again, no water adduct or corresponding transition state could be optimized for addition a water to the $PuO(OH)_5$ intermediate to form $Pu(OH)_7$.

Hydration vs full hydrolysis products For all of the high oxidation state oxo or oxo/hydroxo initial complexes, formation of the first water adduct is an exothermic process. The energetics for the closed shell species are all ~ -22 kcal/mol, independent of the formal oxidation state. The open shell species show more variation with PaO_2 and UO_2 having values of *ca.* -17 kcal/mol and $UO_2(OH)$ having a value of -25 kcal/mol (Table 3). The addition of the second H_2O releases

essentially the same amount of energy for all the actinides and ranges from -19 to -21 kcal/mol, just about double the energy to add one H_2O, again with some of the open shell species being slightly less exothermic, as low as -12 kcal/mol for the second water addition (NpO_3). The addition of the third H_2O follows the same pattern of being independent of actinide.

The An-OH_2 bond distances for 1 water and 2 water hydration are reported in Table 1. Excluding ThO_2, there are very small changes in the An-OH_2 bond distances with the actinide for both 1 water and 2 water hydration products and the 2 water product has slightly longer An-OH_2 bond distances than the 1 water hydration product.

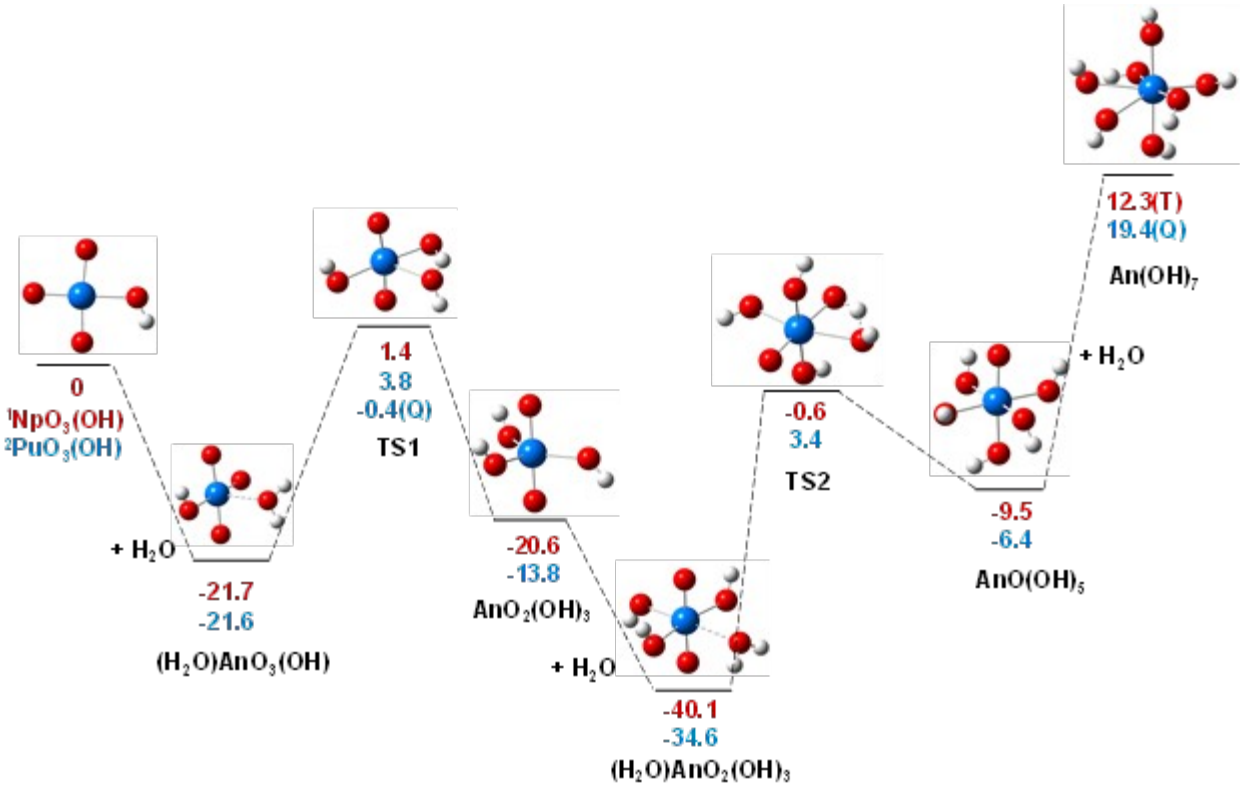

Figure 7. Reaction coordinate energies (ΔH_{298K}) in kcal/mol at CCSD(T)/aD-DK for $^1NpO_3(OH)$ and $^2PuO_3(OH)$ hydrolysis. T = Triplet, Q = Quartet. Actinide in blue, Oxygen in red and Hydrogen white.

Table 3. Overall reaction energies (ΔH_{298K}) in kcal/mol at the CCSD(T)/aD-DK level.

Initial Species	1 H_2O			2 H_2O				3 H_2O			
	ΔH^a	Chemisorb[b]	ΔH^c	Physisorb	ΔH^a	Chemisorb[b]	ΔH^c	Physisorb	ΔH^a	Chemisorb[b]	ΔH^c
ThO_2	-21.5	$ThO(OH)_2$	-60.0	$(H_2O)_2ThO_2$	-42.7	$Th(OH)_4$	-123.6				
PaO_2	-17.8	$PaO(OH)_2$	-23.5	$(H_2O)_2PaO_2(C_{2v})$	-36.1	$Pa(OH)_4$	-75.0				
UO_2	-16.3	$UO(OH)_2$	-30.7	$(H_2O)_2UO_2(C_2)$	-31.8	$U(OH)_4$	-78.9				
$PaO_2(OH)$	-21.9	$PaO(OH)_3$	-42.8	$(H_2O)_2PaO_2(OH)$	-41.8	$Pa(OH)_5$	-67.7				
$UO_2(OH)$	-25.1	$UO(OH)_3$	-16.3	$(H_2O)_2UO_2(OH)$	-42.3	$U(OH)_5$	-55.2				
UO_3	-22.2	$UO_2(OH)_2$	-46.0	$(H_2O)_2UO_3$	-42.6	$UO(OH)_4$	-54.8	$(H_2O)_3UO_3$	-58.4	$U(OH)_6$	-60.2
NpO_3	-22.4	$NpO_2(OH)_2$	-39.3	$(H_2O)_2NpO_3$	-34.4	$NpO(OH)_4$	-36.8	$(H_2O)_3NpO_3$	-58.9	$Np(OH)_6$	-52.0
$NpO_3(OH)$	-21.7	$NpO_2(OH)_3$	-20.6	$(H_2O)_2NpO_3(OH)$	-41.1	$NpO(OH)_5$	-9.5	$(H_2O)_3NpO_3(OH)$	-	$Np(OH)_7$	12.3
$PuO_3(OH)$	-21.6	$PuO_2(OH)_3$	-13.8	$(H_2O)_2PuO_3(OH)$	-40.9	$PuO(OH)_5$	-6.4	$(H_2O)_3PuO_3(OH)$	-	$Pu(OH)_7$	19.4

[a] Physisorption of H_2O enthalpy

[b] Chemisorbed species after addition of n H_2O, for n = 1, 2 or 3.

[c] Chemisorption of H_2O enthalpy

The hydrolysis of ThO_2 is characteristic of transition metal oxide hydrolysis[73] with the energy to form the hydrolysis product, $Th(OH)_4$, almost 3 times more exothermic than for formation of the hydration product, $(H_2O)_2ThO_2$ (Table 3). The complete hydrolysis of $PaO_2(OH)$ to $Pa(OH)_5$ is preferred over the hydration product, $(H_2O)_2PaO_2(OH)$, although the hydrolysis product is not as exothermic as for Th supporting our previous results for PaO_2^+ that the formal Pa(V) oxidation state is more transition metal-like than actinide-like.[73] For UO_3, the hydrolysis product, $U(OH)_6$, and hydration product, $(H_2O)_3UO_3$, are essentially isoenergetic. For NpO_3, the hydration product, $(H_2O)_3NpO_3$, is preferred over the hydrolysis product, $Np(OH)_6$. For $NpO_3(OH)$, a maximum of 2 water molecules can bind to Np(VII) in the first solvation shell and the hydration product is clearly preferred over its corresponding hydrolysis product, $NpO(OH)_5$. Reaction energetics similar to $NpO_3(OH)$ were calculated for the corresponding Pu^{VII} compound, $PuO_3(OH)$.

Natural Population Analysis The NPA values from the Natural Bond Orbitals are given in the Supporting Information. The 6p populations are not quite fully populated with 6 electrons. The amount of population in the 6p orbitals decreases as the formal oxidation state increases. For ThO_2, the Th has a positive charge of +2.5 e which increases as water molecules are added and converted to hydroxides. The increase in positive charge comes with a loss of electronic occupation from the 5f and 6d orbitals. For $^2PaO_2$, the charge on the Pa is about 0.4 e less than on the Th in ThO_2. As H_2O molecules are added and converted to hydroxides, the positive charge on the Pa increases as for ThO_2. The unpaired spin in $^2PaO_2$ is mostly localized in the 7s with a small amount in the 6d and there are about 1.3 e doubly occupied electrons in the 5f and 0.9 electrons

doubly occupied in the 6d. The amount of spin on the 7s decreases and the amount of spin in the 6d increases on addition of the first H_2O molecule.

At $PaO(OH)_2$, there is a significant decrease in the 5f population. Addition of the second H_2O leads to a transfer of spin from the 7s and 6d to the 5f so that the electron configuration is predominantly $5f^1$. The population in the 5f almost doubles from that in $PaO(OH)_2$ and the number of electrons in the 7s drops to under 0.1 e. The 6d orbital population also is decreasing as H_2O molecules are added as was found for ThO_2. However, after the dip in the 5f population at $PaO(OH)_2$, the amount of 5f character remains approximately constant with about 0.3 in backbonding coupled with the approximately 1 unpaired electron on the Pa. In many ways $^3UO_2$ is like $^2PaO_2$. The initial state is $7s^15f^1$ and this converts to $7f^2$ during $UO(OH)_2$ formation, at the first transition state. In this case, the 5f population increases at TS1 and the 7s population drops almost to zero. As for the other two oxides already discussed, the 6d population deceases on H_2O addition, but there is still a significant 6d population even for $U(OH)_4$.

As would be expected, there is a larger positive charge on the Pa, in $PaO(OH)_2$ than on the Pa in PaO_2. The positive charge on the Pa increases with addition of H_2O and conversion to hydroxides. The amount of spin paired backbonding to the 5f decreases with H_2O addition but the amount of 6d backbonding does not decrease by very much, and there is larger 6d occupancy as compared to PaO_2. For $^2UO_2(OH)$, the positive charge on the U increases as H_2O is added as found for $PaO_2(OH)$. The spin remains in a 5f orbital throughout the reaction coordinate. There is a slight dip in the 5f unpaired spin for $UO(OH)_3$. The amount of 5f orbital backbonding decreases with H_2O addition and the 6d backbonding electrons show only minor variations. As found for many of the other compounds, the 5f population decreases as H_2O molecules are added.

The addition of H_2O molecules to UO_3 follows the trends discussed above with an increase in positive charge and decreases in the 5f and 6d backbonding electron populations. The maximum positive charge peaks at $UO(OH)_4$. The same trends are found for NpO_3 with the unpaired electrons remaining in the 5f orbitals on the Np. There is less increase in the positive charge on the Np as H_2O molecules are added. The same peak for the maximum positive charge occurs for $NpO(OH)_4$.

The positive charge on the Np in $NpO_3(OH)$ is almost the same as in NpO_3. There is less variation in the positive charge with addition of H_2O and the peak in the positive charge is at $NpO_2(OH)_3$. There is essentially no variation in the 6d population and the population in the 5f orbitals decrease somewhat until $NpO_2(OH)_3$ with very small changes for additional H_2O molecules. For the reaction coordinate for $PuO_3(OH)$, the unpaired spin remains in the 5f orbitals with the two exceptions noted above where the ground states are quartets with 2 unpaired 5f electrons on Pu and one unpaired spin on one or two OH groups. The charges on the Pu follow the same patterns as for the Np on the $NpO_3(OH)$ reaction coordinate. The high spin ground state species have slightly more positive charge on the An.

The physiosorbed water complexes have positive An charges similar to their corresponding initial oxo/hydroxo species and these charges slightly decrease as more water molecules are added. The only exception is observed for ThO_2 where the Th charges on the physiosorbed water complexes increase relative to the initial ThO_2. There are no significant changes in the orbital occupation from 1 to 2 to 3 physiosorbed water complexes.

Assessment of hydrolysis transformations The chemisorption hydrolysis processes correspond to conversion of an oxo to two hydroxo ligands, with no change in the formal actinide oxidation

state. The hydrolysis energy reflects changes in bonding, with greater exothermicity indicating higher relative stability of the created hydroxo bonds versus the disrupted oxo. The computed hydrolysis energies and actinide charges are summarized in Table 4 and Figures 8 and 9. The three basic types of oxo ligands in initial and partially hydrolyzed species are classified as follows: an "equatorial" oxo is approximately *cis* to two "axial" oxos, as in AnO_3; "axial" actinyl-like oxos are approximately *trans* to one another, as in $AnO_2(OH)_2$; and a "terminal" oxo is the final oxo that is hydrolyzed, as in $AnO(OH)_4$. The hydrolysis reactions are accordingly classified in Figure 8 based on the type of oxo hydrolyzed: ***H-Eq*** for equatorial oxo hydrolysis; ***H-Ax*** for axial oxo hydrolysis; and ***H-Term*** for terminal oxo hydrolysis.

Table 4. Charges on actinides and hydrolysis enthalpies in kcal/mol at the CCSD(T)/aD-DK level.

Initial Species		1st Hydrolysis[c]		2nd Hydrolysis[d]		3rd Hydrolysis[e]	
	q(An)[a]	ΔH_{298K}	q(An)[b]	ΔH_{298K}	q(An)[b]	ΔH_{298K}	q(An)[b]
ThO_2	2.500	-60.0	2.807	-63.6	2.990	-	-
PaO_2	2.102	-23.5	2.493	-51.5	2.824	-	-
UO_2	1.970	-30.7	2.583	-48.2	2.755	-	-
$PaO_2(OH)$	2.818	-42.8	3.068	-24.9	3.064	-	-
$UO_2(OH)$	2.651	-16.3	2.893	-38.9	2.901	-	-
UO_3	2.626	-46.0	2.776	-8.8	2.873	-5.4	2.813
NpO_3	2.409	-39.3	2.586	2.5	2.686	-15.2	2.559
$NpO_3(OH)$	2.406	-20.6	2.548	11.1	2.459	21.8	2.462
$PuO_3(OH)$	2.269	-13.8	2.336	7.4	2.262	25.8	2.363

[a] Charge on actinide in initial species $AnO_m(OH)_n$.
[b] Charge on actinide in hydrolysis product.
[c] 1st Hydrolysis reaction: $AnO_m(OH)_n + H_2O \rightarrow AnO_{m-1}(OH)_{n+2}$.
[d] 2nd Hydrolysis reaction: $AnO_{m-1}(OH)_{n+2} + H_2O \rightarrow AnO_{m-2}(OH)_{n+4}$.
[e] 3rd Hydrolysis reaction: $AnO_{m-2}(OH)_{n+4} + H_2O \rightarrow AnO_{m-3}(OH)_{n+6}$.

Referring to Figure 8a, the initial hydrolysis reaction ***H-Ax*** is very exothermic for ThO_2, which is highly bent and has longer bonds than the other AnO_2. The absence of a near-linear

actinyl moiety in ThO_2 is evidently manifested as a particularly favorable oxo-to-hydroxo conversion. For linear PaO_2 and UO_2, and the slightly bent (168^0) dioxo moiety in $UO_2(OH)$, disruption of the actinyl-like unit by hydrolysis reaction ***H-Ax*** is significantly less exothermic than for ThO_2. In comparison, reaction ***H-Ax*** of the dioxo in $PaO_2(OH)$, which is bent to 161^0, has intermediate exothermicity between highly bent ThO_2 and linear PaO_2. These results suggest that resistance of the AnO_2 moiety to disruption increases as it becomes more linear actinyl-like.

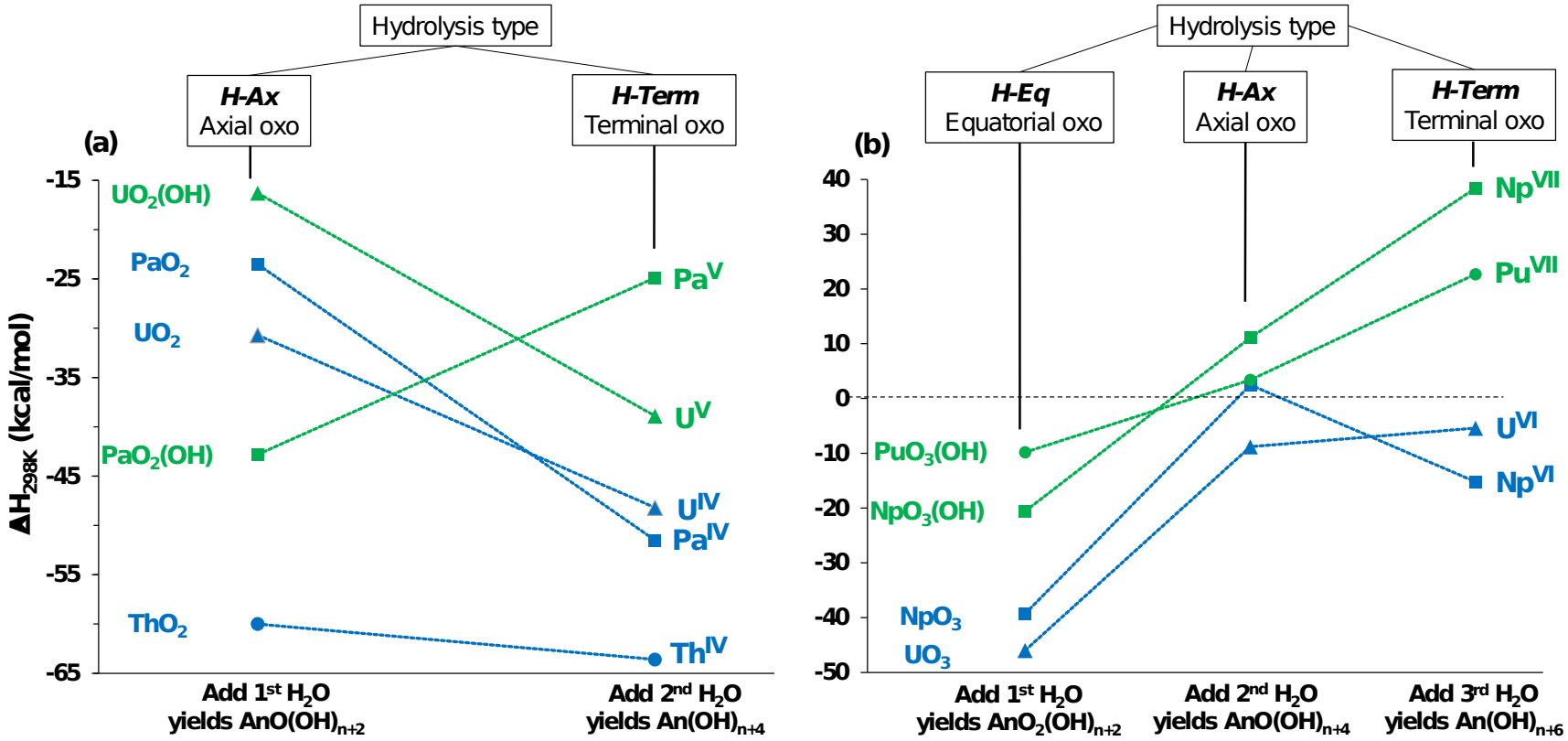

Figure 8. Enthalpies for sequential hydrolytic addition of H_2O starting with the indicated species in oxidation states: (a) An^{IV} and An^{V}; and (b) An^{VI} and An^{VII}. The hydrolysis processes are classified according to the type of hydrolyzed oxo: Equatorial (***H-Eq***), Axial (***H-Ax***), or Terminal (***H-Term***).

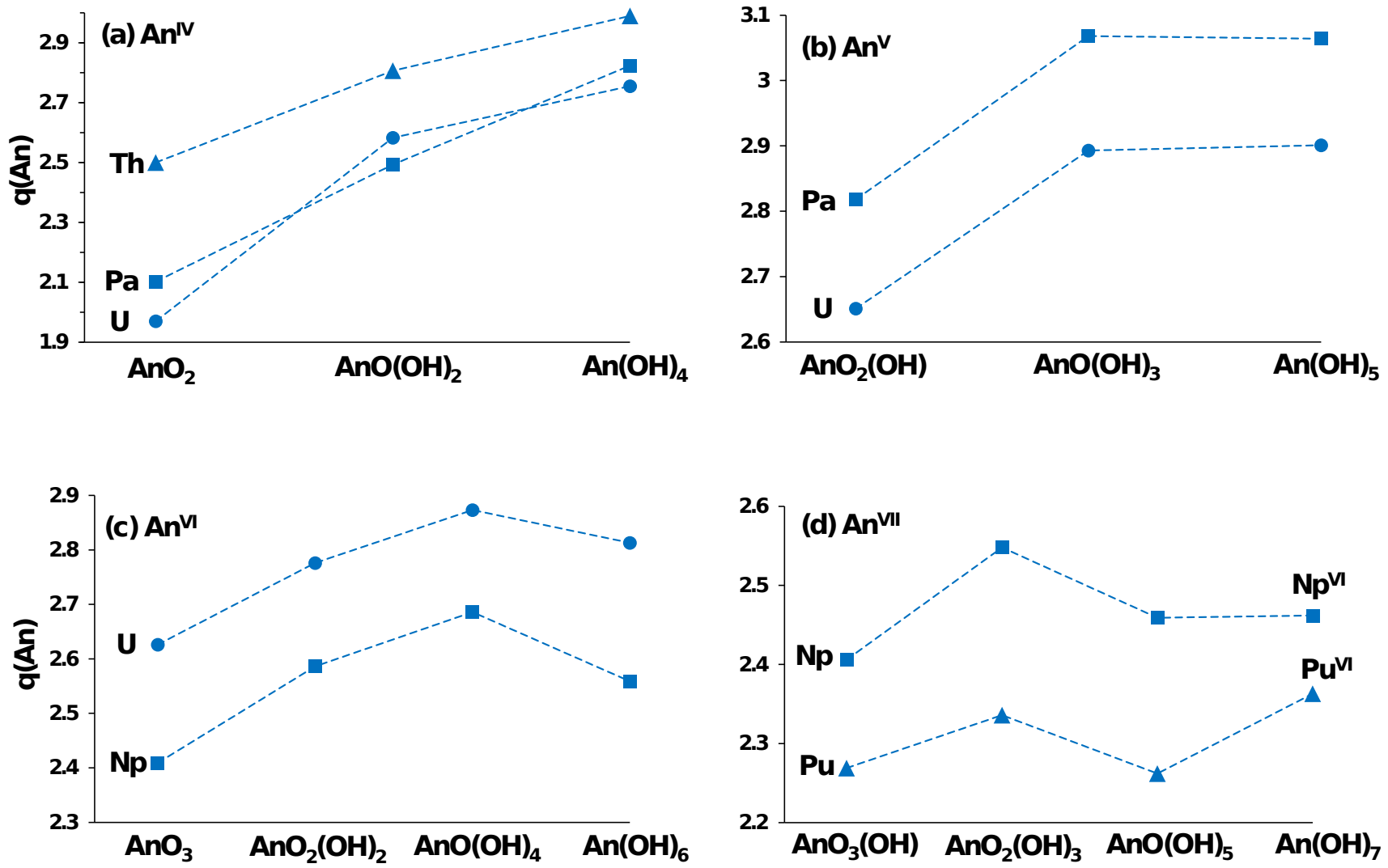

Figure 9. Charge on the actinide for the studied oxides, oxide hydroxides, and hydroxides in oxidation states: (a) An^{IV}; (b) An^{V}; (c) An^{VI}; and (d) An^{VII}. Note that for $An(OH)_7$, it is An^{VI}. See the text.

The ***H-Term*** reactions for $ThO(OH)_2$, $PaO(OH)_2$, $UO(OH)_2$ and $UO(OH)_3$ are more exothermic than for the corresponding ***H-Ax***, indicating easier disruption of the terminal oxo than for conversion to the actinyl-like moiety. In contrast, reaction ***H-Term*** for $PaO(OH)_3$ is remarkably significantly less exothermic, i.e., less favorable, than reaction ***H-Ax*** for $PaO_2(OH)$. To understand this seemingly odd relationship for Pa^V, it is noted that the sum of the energies for reaction ***H-Ax*** + reaction ***H-Term*** is similar for $UO_2(OH)$ and $PaO_2(OH)$ (-55 and -68 kcal/mol, respectively). The distribution of energies for Pa^V hydrolysis—highly exothermic reaction ***H-Ax*** and mildly exothermic reaction ***H-Term***—may relate to a particularly stable initial reaction ***H-Ax*** hydrolysis product, $PaO(OH)_3$, which has a C_{3v}-like "piano stool" structure. In contrast, the structure of $UO(OH)_3$ has lower C_{2v}-like symmetry, with one of the three hydroxo ligands retaining some "axial" character from the dioxo precursor (see structures in Figures 3 and 4). In essence, the differing hydrolysis character of Pa^V versus U^V appears to reflect greater resistance of the uranyl(V) moiety towards disruption. An essentially equivalent perspective is that the distinctively favorable reaction ***H-Eq*** for $PaO_2(OH)$ reflects more ionic character and less bond disruption upon hydrolysis of the protactinyl(V) moiety.

Considering the species in Figure 8b with high oxidation states An^{VI} and An^{VII}, the ***H-Eq*** reactions for UO_3 and NpO_3 are highly exothermic whereas all the other hydrolyses are in the range of moderately exothermic to substantially endothermic. A given type of hydrolysis—reaction ***H-Eq***, ***H-Ax*** or ***H-Term***—is less exothermic for An^{VII} versus An^{VI}, which may relate to decreasing bond ionicity with increasing oxidation state because lower ionicity for higher oxidation states should generally favor more covalent oxo versus ionic hydroxo bonds. Another factor that should generally disfavor hydrolysis of higher oxidation states is increased repulsion

between hydroxide ligands as the actinide coordination increases, an effect greatest for the An^{VII} species. For all four considered An^{VI} and An^{VII} systems, destruction of the actinyl-like moiety in hydrolysis reaction ***H-Ax*** is less exothermic than for the equatorial oxo in reaction ***H-Eq***, which is as expected based on the high stability of the dioxo unit. For the two An^{VI}, reaction ***H-Term*** is at a roughly similar energy to reaction ***H-Ax***, whereas reaction ***H-Term*** for An^{VII} is substantially less favorable than ***H-Ax***. Moreover, the ***H-Term*** reaction energetically favors high spin ground state species with An^{VI}, not An^{VII}, as seven OH groups are not strong enough ligands to stabilize the +VII oxidation state on the actinides. The results that these ***H-Term*** reactions are not more favorable than reaction ***H-Ax*** likely also reflects repulsion between the ligands in the high-coordinate products, particularly in $An(OH)_7$.

Although the computed actinide charge, q(An), is not a physically observable property, it provides a useful basis for comparisons. Values of q(An) are summarized in Table 4 and Figure 9. For homoleptic species like UO_2 and $Th(OH)_4$, q(An) indicates the metal-to-ligand charge transfer for equivalent ligands, which in turn reveals the An-OH bond ionicity. For heteroleptic species like $PaO_2(OH)$ and $Pa(OH)_5$, q(An) does not differentiate charge transfer to the non-equivalent ligands, instead indicating the overall ionic character of the molecule. For each of the three An^{IV} species—AnO_2, $AnO(OH)_2$ and $An(OH)_4$—the values for $q(Pa^{IV})$ and $q(U^{IV})$ are similar to one another, and lower than $q(Th^{IV})$. More generally, for all oxidation states, the lighter of the neighboring actinides has the higher charge: $q(Th^{IV}) > q(Pa^{IV})$; $q(Pa^{V}) > q(U^{V})$; $q(U^{VI}) > q(Np^{VI})$; $q(Np^{VII}) > q(Pu^{VII})$. These relationships suggest that bond ionicity, as indicated by charge transfer, decreases from lighter to heavier actinides; an equivalent statement is that bond covalency increases across the actinide series.

Figure 9 shows the effect of hydrolysis of the An^{IV} on q(An), which increases from AnO_2 to $AnO(OH)_2$ to $An(OH)_4$. An analogous trend of continuously increasing q(An) upon hydrolysis and increasing coordination is not exhibited for higher oxidation states. For An^{V}, q(An) increases from $AnO_2(OH)$ to $AnO(OH)_3$ but then remains nearly constant to $An(OH)_5$. For An^{VI}, there is an increase in q(An) for the first two hydrolyses—from AnO_3 to $AnO_2(OH)_2$ and also to $AnO(OH)_4$—but a decrease for the final hydrolysis to $An(OH)_6$. For An^{VII}, q(An) increases for the initial hydrolysis from $AnO_3(OH)$ to $AnO_2(OH)_3$, but then decreases to $AnO(OH)_5$. The cases of decreasing q(An) upon hydrolysis indicate net charge transfer from the ligands to the metal center when an oxo is converted to two hydroxos with a concomitant increase in actinide coordination. Such a reversal of charge transfer—essentially ligand-to-metal rather than more typical metal-to-ligand transfer—appears for coordination number above four or five. For example, the five ligands in $UO(OH)_4$ (q(U) = 2.87) withdraw more charge than the six ligands in $U(OH)_6$ (q(U) = 2.81), with the overall bonding in the latter thus less ionic and implicitly more covalent.

In analogy with the curious ligand-to-metal charge transfer effect noted above for fixed oxidation states like U^{VI}, the seemingly counterintuitive effect of decreasing positive actinide charge upon addition of formally electron-withdrawing ligands also appears for different oxidation states. For example, the charge q(U) intuitively increases from 2.76 in $U^{IV}(OH)_4$ to 2.90 in $U^{V}(OH)_5$, but it then decreases to 2.81 in $U^{VI}(OH)_6$. The effect is more obvious upon considering the average charges on the hydroxide ligands in the fully hydroxylated species, $An(OH)_n$. The average hydroxide charge parameter is here simply defined as: $q_{AV}(OH) = -q(An)/n$. Although the charge on all hydroxides is not necessarily equal to the average for a heteroleptic species like $Pa(OH)_5$, $q_{AV}(OH)$ is nonetheless a useful indicator of the typical bond character in

such species. The parameter $q_{AV}(OH)$ becomes substantially less negative with increasing hydroxylation of uranium: the values of $q_{AV}(OH)$ are -0.69 in $U(OH)_4$, -0.58 in $U(OH)_5$ and -0.47 in $U(OH)_6$. A similar charge comparison is shown in Figure 10a for species with different actinides in their

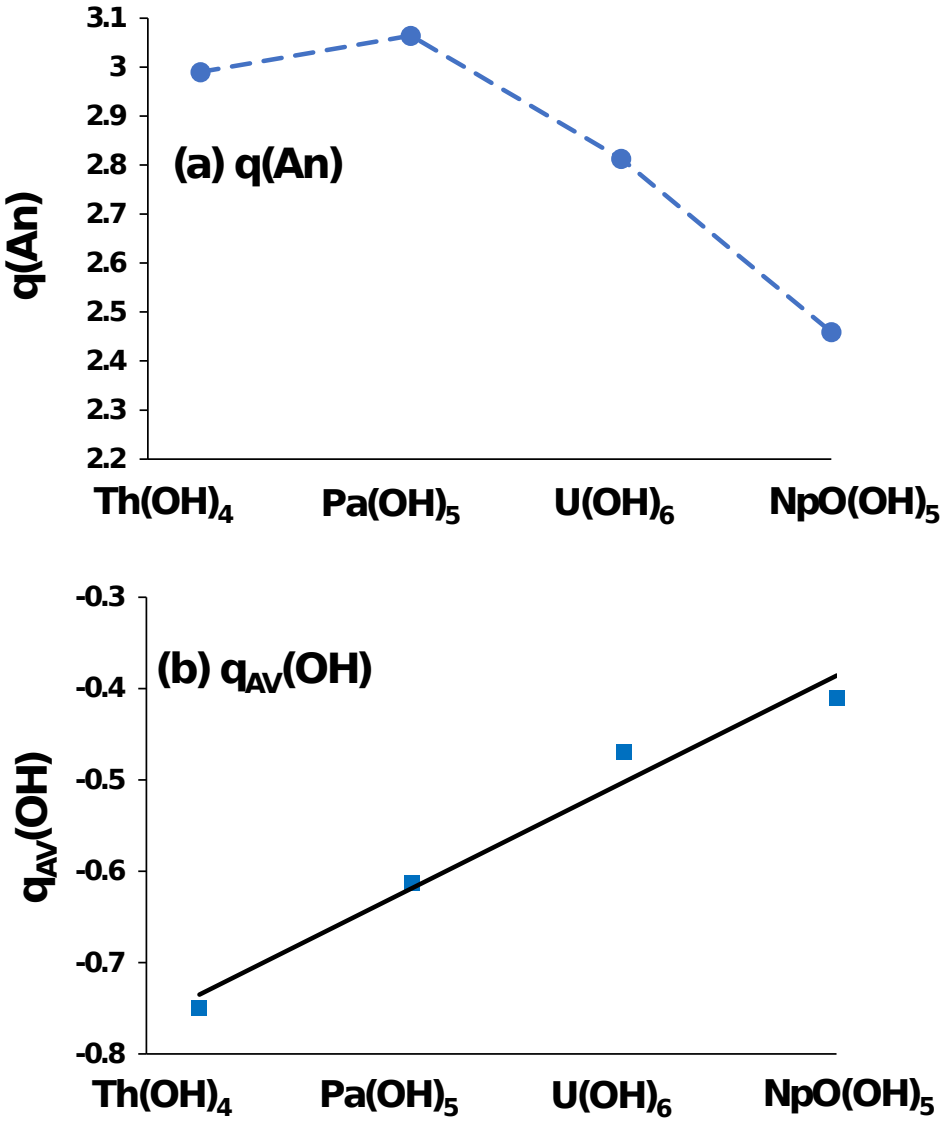

Figure 10. Charges for fully hydrolyze to highest oxidation state products: $Th(OH)_4$, $Pa(OH)_5$, $U(OH)_6$ and $NpO(OH)_5$: (a) Charge on the actinide, q(An). (b) Average charge on the OH ligands in $An(OH)_n$ ($q_{AV}(OH) = -q(An)/n$).

highest oxidation states, Th^{IV}, Pa^{V}, U^{VI} and Np^{VII}. There is a slight increase in q(An) from $Th(OH)_4$ to $Pa(OH)_5$, followed by substantial decreases to $U(OH)_6$ and then to $NpO(OH)_5$. These relationships indicate less net charge transfer from the actinide upon addition of the sixth and seventh hydroxide ligands. Considering the corresponding $q_{AV}(OH)$ in Figure 10b, the hydroxide charges become substantially less negative as the oxidation state increases: the $q_{AV}(OH)$ are -0.74 in $Th(OH)_4$; -0.61 in $Pa(OH)_5$; -0.47 in $U(OH)_6$ and -0.41 in $NpO(OH)_5$. Trends in charge transfer can be summarized as follows: For increasing coordination at constant oxidation state, such as U^{VI}, and for increasing both coordination and oxidation state, such as from Th^{IV} to Np^{VII}, the ionicity of each An-OH bond decreases and bond covalency thus increases.

Conclusions

Hydrolysis reaction energetics for oxo and oxo-hydroxo actinide monomers have been calculated for the actinides An =Th- Pu in high oxidation states at the CCSD(T) level. Each reaction is initiated by formation of a Lewis acid/base adduct with H_2O followed by a proton transfer to form a dihydroxide molecule and repeated until all oxo groups are hydrolyzed. $Th^{IV}O_2$ proved to be the species most capable of easily undergoing hydrolysis and the energetics are similar to those for transition metal oxides. The amount of energy released on formation of the fully hydrolyzed molecule $Th(OH)_4$ is almost twice that of the corresponding Pa or U species. The physisorption for each H_2O addition was predicted to be exothermic and approximately the same, *ca.* -20 kcal/mol, with small energy changes for the open shell species. For the early actinide oxo and oxo/hydroxo species with An in the +IV and +V oxidation states, hydrolysis products are preferred energetically over the hydration products. The An in the +VI oxidation state are a turning point where for UO_3, the hydrolysis product, $U(OH)_6$, and hydration product, $(H_2O)_3UO_3$, are essentially isoenergetic and for NpO_3, the hydration product, $(H_2O)_3NpO_3$, is

preferred over the hydrolysis product, $Np(OH)_6$. For An in the +VII oxidation state, the hydration products are preferred and only 2 waters can bind $An^{VII}O_3(OH)$. The complete hydrolysis process is calculated to be endothermic.

For the An in formal oxidation states +IV - +VI, especially for the closed shell molecules, there is a large positive charge on the An of the initial species which increases as water molecules are added and converted to hydroxides. As this charge increases, there is a decrease in the 5f and 6d backbonding electron populations on the An. There is a decrease in the An charge from closed shell to open shell species. For An in the +VII oxidation state, there is less variation in the positive charge with addition of H_2O and there is essentially no variation in the 6d population and the population in the 5f orbitals.

The reaction energies and NBO charges elucidate the nature of these hydrolysis processes. Initial hydrolysis of $An^{IV}O_2$ destroys the actinyl-like moiety and is thus energetically less favorable than hydrolysis of the terminal oxo in $O=An^{IV}(OH)_2$. Whereas $U^{V}O_2(OH)$ similarly exhibits more favorable terminal versus axial hydrolysis, the dioxo moiety in $Pa^{V}O_2(OH)$ is remarkably more easily hydrolyzed than the terminal oxo in $O=Pa^{V}(OH)_3$. For the An^{VII} species, hydrolysis of the final terminal oxo is endothermic and the An oxidation state is +VI leading to a high spin triplet for Np and a quartet for Pu with a spin on two OH groups in the $An(OH)_7$. Thus, the OH groups are not strong enough ligands to stabilize the +VII oxidation state, so the molecule does not have full ionic bonding. In addition, repulsion between the more crowded ligands could also contribute to the destabilization of $An(OH)_7$. The actinide charges and bond ionicities generally decrease across the series, such that $Np^{VI}O_3$ is less ionic than $U^{VI}O_3$. Ionic character also decreases as the oxidation state and coordination number increase, with the An-

OH bonds in $Th^{IV}(OH)_4$ the most ionic and those in $Np^{VII}O(OH)_5$ the least ionic, to wit the most covalent.

Author Information

Corresponding Author: David A. Dixon. email: dadixon@ua.edu

ORCID:

Monica Vasiliu: 0000-0001-7573-4787

David A. Dixon: 0000-0002-9492-0056

John K. Gibson: 0000-0003-2107-5418

Acknowledgement. This work was supported by the U.S. Department of Energy, Office of Science, Office of Basic Energy Sciences, Chemical Sciences, Geosciences, and Biosciences Division, Heavy Element Chemistry Program, at The University of Alabama under Grant No. DE-SC0018921 and at the Lawrence Berkeley National Laboratory under Contract DE-AC02-05CH11231. D.A.D. thanks the Robert Ramsay Fund at The University of Alabama.

Supporting Information Complete references for 44 and 55. Additional reaction energetics. NBO/NPA analysis. $AnO_3(OH)$ high-low spin energy gaps. Cartesian coordinates in Å for B3LYP optimized geometries

References

[1] Wang, T.-H.; Fang, Z.; Gist, N. W.; Li, S.; Dixon, D. A.; Gole, J. L. Computational Study of the Hydrolysis Reactions of the Ground and First Excited Triplet States of Small TiO_2 Nanoclusters. *J. Phys. Chem. C* **2011**, *115*, 9344-9360.

[2] Fang, Z.; Outlaw, M. D.; Smith, K. K.; Gist, N. W.; Li, S.; Dixon, D. A.; Gole, J. L., Computational Study of the Hydrolysis Reactions of Small MO_2 (M = Zr and Hf) Nanoclusters with Water. *J. Phys. Chem. C* **2012**, *116*, 8475-8492.

[3] Natrajan, L. S; Swinburne, A. N; Andrews, M. B; Randall S.; Heath, S. L. Redox and Environmentally Relevant Aspects of Actinide (IV) Coordination Chemistry. *Coordin. Chem. Rev*. **2014,** *266-267*, 171-193.

[4] Choppin, G. R., Actinide Speciation in the Environment. *J. Radioanal. Nucl. Ch*. **2007,** *273*, 695-703.

[5] Crandall, H. W. The Formula of Uranyl Ion. *J. Chem. Phys.* **1949**, *17*, 602−606.

[6] Gordon, G.; Taube, H. J. The Uranium(V)-Catalysed Exchange Reaction Between Uranyl Ion and Water in Perchloric Acid Solution. *Inorg. Nucl. Chem.* **1961**, *16*, 272−278.

[7] Clark, D. L.; Conradson, S. D.; Donohoe, R. J.; Keogh, D. W.; Morris, D. E.; Palmer, P. D.; Rogers, R. D.; Tait, C. D. Chemical Speciation of the Uranyl Ion under Highly Alkaline Conditions. Synthesis, Structures, and Oxo Ligand Exchange Dynamics. *Inorg. Chem.* **1999**, *38*, 1456−1466.

[8] Szabo, Z.; Grenthe, I. Reactivity of the "yl"-Bond in Uranyl(VI) Complexes. 1. Rates and Mechanisms for the Exchange between the *trans*-dioxo Oxygen Atoms in $(UO_2)_2(OH)_2^{2+}$ and Mononuclear $UO_2(OH)_n^{2-n}$ Complexes with Solvent Water. *Inorg. Chem.* **2007**, *46*, 9372−9378.

[9] Szabo, Z.; Grenthe, I. On the Mechanism of Oxygen Exchange Between Uranyl(VI) Oxygen and Water in Strongly Alkaline Solution as Studied by ^{17}O NMR Magnetization Transfer. *Inorg. Chem.* **2010**, *49*, 4928−4933.

[10] Fortier, S.; Hayton, T. W. Oxo Ligand Functionalization in the Uranyl Ion (UO_2^{2+}). *Coord. Chem. Rev.* **2010**, *254*, 197−214.

[11] Rabideau, S. W.; Masters, B. J. Oxygen Exchange Reactions of Plutonium Ions in Solution. *J. Phys. Chem.* **1963**, *67*, 318−323.

[12] Rabideau, S. W. The Oxygen Exchange Reactions of NpO_2^{+2} and NpO_2^{+} with Water. *J. Phys. Chem.* **1963**, *67*, 2655−2659.

[13] Wahlin, P.; Danilo, C.; Vallet, V.; Réal, F.; Flament, J. P.; Wahlgren, U. An Investigation of the Accuracy of Different DFT Functionals on the Water Exchange Reaction in Hydrated Uranyl(VI) in the Ground State and the First Excited State. *J. Chem. Theory Comput.* **2008**, *4*, 569−577.

[14] Réal, F.; Vallet, V.; Wahlgren, U.; Grenthe, I. Ab Initio Study of the Mechanism for Photoinduced Yl-Oxygen Exchange in Uranyl(VI) in Acidic Aqueous Solution. *J. Am. Chem. Soc.* **2008**, *130*, 11742−11751.

[15] Shamov, G. A.; Schreckenbach, G. Theoretical Study of the Oxygen Exchange in Uranyl Hydroxide. An Old Riddle Solved? *J. Am. Chem. Soc.* **2008**, *130*, 13735−13744.

[16] Schreckenbach, G.; Shamov, G. A. Theoretical Actinide Molecular Science. *Acc. Chem. Res*. **2010**, *43*, 19−29.

[17] Bühl, M.; Schreckenbach, G. Oxygen Exchange in Uranyl Hydroxide via Two "Nonclassical" Ions. *Inorg. Chem*. **2010**, *49*, 3821−3827.

[18] Bühl, M.; Wipff, G. Insights into Uranyl Chemistry from Molecular Dynamics Simulations. *ChemPhysChem*. **2011**, *12*, 3095−3105.

[19] Tsushima, S. "yl"-Oxygen Exchange in Uranyl(VI) Ion: A Mechanism Involving $(UO_2)_2(\mu\text{-}OH)_2^{2+}$ via $U–O_{yl}–U$ Bridge Formation. *Inorg. Chem*. **2012**, *51*, 1434−1439.

[20] Rios, D.; Michelini, M. d. C.; Lucena, A. F.; Marçalo, J.; Gibson J. K. On the Origins of Faster Oxo Exchange for Uranyl(V) versus Plutonyl(V). *J. Am. Chem. Soc.* **2012**, *134*, 15488−15496.

[21] Dau, P. D.; Wilson, R. E.; Gibson J. K. Elucidating Protactinium Hydrolysis: The Relative Stabilities of $PaO_2(H_2O)^+$ and $PaO(OH)_2^+$. *Inorg. Chem.* **2015**, *54*, 7474–7480.

[22] Dixon, D. A.; Feller, D.; Peterson. K. A. A Practical Guide to Reliable First Principles Computational Thermochemistry Predictions Across the Periodic Table. in *Annual Reports in Computational Chemistry*, *Vol. 8*, Ed Wheeler, R. A.; Section Ed. Tschumper, G. S.; Elsevier: Amsterdam, 2012, Ch. 1, pp. 1-28.

[23] Feller, D.; Peterson, K. A.; Dixon, D. A. Further Benchmarks of a Composite, Convergent, Statistically-Calibrated Coupled Cluster-Based Approach for Thermochemical and Spectroscopic Studies. *Mol. Phys.* **2012**, *110*, 2381–2399.

[24] Peterson, K. A.; Feller, D.; Dixon, D. A. Chemical Accuracy in Ab Initio Thermochemistry and Spectroscopy: Current Strategies and Future Challenges. *Theor. Chem. Acc.* **2012**, *131*, 1079.

[25] Feller, D.; Peterson, K. A.; Dixon, D. A. The Impact of Larger Basis Sets and Explicitly Correlated Coupled Cluster Theory on the Feller-Peterson-Dixon Composite Method. in *Annual Reports in Computational Chemistry*, Vol. 12, Ed. Dixon, D. A. Elsevier: Amsterdam, 2016, pp. 47-78.

[26] Vasiliu, M.; Peterson, K. A.; Gibson, J. K.; Dixon, D. A. Reliable Potential Energy Surfaces for the Reactions of H_2O with ThO_2, PaO_2^+, UO_2^{2+}, and UO_2^{2+}. *J. Phys. Chem. A* **2015**, *119*, 11422−11431.

[27] Katharina Boguslawski, K.; Réal, R.; Tecmer, P.; Duperrouzel, C.; Severo Pereira Gomes, A.; Legeza, O.; Ayersd, P. W.; Vallet, V. On the Multi-Reference nature of Plutonium Oxides: PuO_2^{2+}, PuO_2, PuO_3, $PuO_2(OH)_2$. *Phys. Chem. Chem. Phys.* **2017**, *19*, 4317-4329.

[28] Feng, R.; Vasiliu, M.; Peterson, K. A.; Dixon, D. A. Acidity of $M(VI)O_2(OH)_2$ for M = Group 6, 16, and U as Central Atoms. *J. Phys. Chem. A* **2017**, *121*, 1041−1050.

[29] Gorden, A. E. V.; Mckee M. L., Computational Study of Reduction Potentials of Th^{4+} Compounds and Hydrolysis of $ThO_2(H_2O)_n$, n = 1,2,4. *J. Phys. Chem. A*. **2016**, *41*, 8169-8183.

[30] Tsushima, S. Hydrolysis and Dimerization of Th^{4+} Ion. *J. Phys. Chem. B*. **2008**, *112*, 7080-7085.

[31] de Jong, W. A.; Dau, P. D.; Wilson, R. E.; Marçalo, J.; Van Stipdonk, M. J.; Corcovilos, T. A.; Berden, G.; Martens, J.; Oomens, J.; Gibson, J. K., Revealing Disparate Chemistries of Protactinium and Uranium. Synthesis of the Molecular Uranium Tetroxide Anion, UO_4^-. *Inorg. Chem.* **2017**, *56*, 3686-3694.

[32] Kovács A. Molecular Oxides of High-Valent Actinides. *Struct. Chem.* **2020**, *31*, 1247-1271.

[33] Parr, R. G.; Yang, W. *Density-Functional Theory of Atoms and Molecules*. Oxford University Press: New York, 1989.

[34] Becke, A. D. Density-Functional Thermochemistry. III. The Role of Exact Exchange. *J. Chem. Phys.* **1993**, *98*, 5648-5652.

[35] Lee, C.; Yang, W.; Parr, R. G. Development of the Colle-Salvetti Correlation-Energy Formula into a Functional of the Electron Density. *Phys. Rev. B* **1988**, *37*, 785-789.

[36]Kendall, R. A.; Dunning, T. H., Jr.; Harrison, R. J. Electron Affinities of the First-Row Atoms Revisited. Systematic Basis Sets and Wave Functions. *J. Chem. Phys*. **1992**, *96*, 6796-6806.

[37] Dunning, T.H., Jr. Gaussian Basis Set for use in Correlated Molecular Calculations. I. The Atoms Boron through Neon and Hydrogen. *J. Chem. Phys*. **1989**, *90*, 1007-1023.

[38] Peterson, K. A. Correlation Consistent Basis Sets for Actinides. I. The Th and U Atoms. *J. Chem. Phys.* **2015**, *142*, 074105.

[39] Dolg, M; Cao, X. Accurate Relativistic Small-Core Pseudopotentials for Uranium and First Applications to Uranium Hydride. *J. Phys. Chem. A* **2009**, *113*, 12573-12581.

[40] Weigand, A.; Cao, X.; Hangele, T.; Dolg, M. Relativistic Small-Core Pseudopotentials for Actinium, Thorium, and Protactinium. *J. Phys. Chem. A*. **2014**, *118*, 2519-2530.

[41] Kuchle, W.; Dolg, M.; Stoll, H.; Preuss, H. Energy-Adjusted Pseudopotentials for the Actinides. Parameter sets and Test Calculations for Thorium and Thorium Monoxide. *J. Chem. Phys.* **1994**, 100, 7535-7542.

[42] Cao, X.; Dolg, M. Segmented Contraction Scheme for Small-Core Actinide Pseudopotential Basis sets. *J. Mol. Struc. - THEOCHEM* **2004**, *673*, 203-209.

[43] Cao, X.; Dolg, M.; Stool, M. Valence Basis Sets for Relativistic Energy-Consistent Small-Core Actinide Pseudopotentials. *J. Chem. Phys.* **2003**, *118*, 487-496.

[44] Frisch, M. J.; Trucks, G. W.; Schlegel, H. B.; Scuseria, G. E.; Robb, M. A.; Cheeseman, J. R.; Scalmani, G.; Barone, V.; Petersson, G. A.; Nakatsuji, H.; et al., Gaussian 16, Revision A.03, Gaussian, Inc., Wallingford CT, 2016.

[45] Purvis, G. D., III; Bartlett, R. J. A Full Coupled-Cluster Singles and Doubles Model: The Inclusion of Disconnected Triples. *J. Chem. Phys.* **1982**, *76*, 1910-1918.

[46] Raghavachari, K.; Trucks, G. W.; Pople, J. A.; Head-Gordon, M. A Fifth-order Perturbation Comparison of Electron Correlation Theories. *Chem. Phys. Lett.* **1989**, *157*, 479-483.

[47] Watts, J. D.; Gauss, J.; Bartlett, R. J. Coupled-Cluster Methods with Non-iterative Triple Excitations for Restricted Open-Shell Hartree-Fock and Other General Single-Determinant Reference Functions. Energies and Analytical Gradients. *J. Chem. Phys.* **1993**, *98*, 8718-8733.

[48] Bartlett, R. J.; Musial, M. Coupled-Cluster Theory in Quantum Chemistry. *Rev. Mod. Phys.* **2007**, *79*, 291-352.

[49] Douglas, M.; Kroll, N. M. Quantum Electrodynamical Corrections to the Fine Structure of Helium. *Ann. Phys.* **1974**, *82*, 89-155.

[50] Jansen, G.; Hess, B. A. Revision of the Douglas-Kroll Transformation. *Phys. Rev. A* **1989**, *39*, 6016-6017.

[51] Wolf, A.; Reiher, M.; Hess, B. A. The Generalized Douglas-Kroll Transformation. *J. Chem. Phys.* **2002**, *117*, 9215-9226.

[52] de Jong, W. A.; Harrison, R. J.; Dixon, D. A. Parallel Douglas-Kroll Energy and Gradients in Nwchem: Estimating Scalar Relativistic Effects Using Douglas-Kroll Contracted Basis Sets. *J. Chem. Phys.* **2001**, *114*, 48-53.

[53] De Jong, W. A.; Harrison, R. J.; Dixon, D. A. Parallel Douglas–Kroll Energy and Gradients in NWChem: Estimating Scalar Relativistic Effects Using Douglas–Kroll Contracted Basis Sets. *J. Chem. Phys*. **2001**, *114*, 48-53.

[54] Rulin, F.; Peterson, K.A. Correlation Consistent Basis Sets for Actinides. II. The Atoms Ac and Np – Lr. *J. Chem. Phys.* **2017**, *147*, 084108.

[55] Werner H.-J.; Knowles, P. J.; Knizia, G.; Manby, F. R.; Schütz, M.; Celani, P.; Györffy, W.; Kats, T.; Korona, T.; Lindh, R.; et al. a package of *ab initio* programs, See http://www.molpro.net. Accessed July 1, 2020.

[56] Werner, H.-J.; Knowles, P. J.; Manby, F. R.; Black, J. A.; Doll, K.; Heßelmann, A.; Kats, D.; Köhn, A.; Korona, T.; Kreplin, D. A.; et. al. The Molpro Quantum Chemistry Package. *J. Chem. Phys.* **2020,** *152*, 144107.

[57] Roos, B. O.; Taylor, P. R.; Siegbahn, P. E. M. A Complete Active Space SCF Method (CASSCF) Using a Density-Matrix Formulated Super-CI Approach. *Chem. Phys.* **1980**, *48*, 157-173.

[58] Siegbahn, P. E. M.; Almlöf, J.; Heiberg, A.; Roos, B. O. The Complete Active Space SCF (CASSCF) Method in a Newton-Raphson Formulation with Application to the HNO Molecule. *J. Chem. Phys.* **1981**, *74*, 2384–2396.

[59] Watts, J. D.; Gauss, J.; Bartlett, R. J. Coupled-Cluster Methods with Non-iterative Triple Excitations for Restricted Open-Shell Hartree-Fock and Other General Single-Determinant Reference Functions. Energies and Analytical Gradients. *J. Chem. Phys.* **1993**, *98*, 8718-8733.

[60] Deegan, M. J. O.; Knowles, P. J. Perturbative Corrections to Account for Triple Excitations in Closed and Open Shell Coupled Cluster Theories. *Chem. Phys. Lett.* **1994**, *227*, 321-326.

[61] Rittby, M.; Bartlett, R. J. An Open-Shell Spin-Restricted Coupled Cluster Method: Application to Ionization Potentials in N_2. *J. Phys. Chem*. **1988**, *92*, 3033-3036.

[62] Knowles, P. J.; Hampel, C.; Werner, H.-J. Coupled Cluster Theory for High Spin, Open Shell Reference Wave Functions *J. Chem. Phys.* **1993**, *99*, 5219-5228.

[63] Reed, A. E.; Curtiss, L. A.; Weinhold, F. Intermolecular Interactions from a Natural Bond Orbital, Donor-Acceptor Viewpoint. *Chem. Rev.* **1988**, *88*, 899-926.

[64] Weinhold, F.; Landis, C. R. *Valency and Bonding: A Natural Bond Orbital Donor-Acceptor Perspective*, University Press: Cambridge, U.K., 2005

[65] Glendening, E. D.; Badenhoop, J. K.; Reed, A. E.; Carpenter, J. E.; Bohmann, J. A; Morales, C. M.; Karafiloglou; P.; Landis, C. R.; Weinhold, F. Natural Bond Order 7.0, Theoretical Chemistry Institute, University of Wisconsin, Madison, WI, 2018.

[66] Glendening, E. D.; Landis, C. R.; Weinhold, F. NBO 7.0: New Vistas in Localized and Delocalized Chemical Bonding Theory. *J. Comput. Chem.* **2019**, *40*, 2234-2241.

[67] Jackson, V. E.; Craciun, R.; Dixon, D. A.; Peterson, K. A.; de Jong, W.A. The Vibrational Spectra of UO_2^{2+} Predicted at the CCSD(T) Level. *J. Phys. Chem. A* **2008**, *112*, 4095-4099

[68] Andrews, L.; Gong, Y.; Liang, B.; Jackson, V. E.; Flamerich, R.; Li, S.; Dixon, D. A. Matrix Infrared Spectra and Predicted Properties of Thorium Oxide Species: ThO_x and Th_2O_y. *J. Phys. Chem. A* **2011**, *115*, 14407–14416.

[69] Vasiliu, M.; Peterson, K. A.; Dixon, D. A. Calculated Ionization Potentials of MO_3 and MO_2 for M = U, Mo, W and Nd. *J. Phys. Chem. A* **2020**, *124*, 10, 6913-6919.

[70] Marks, J. H.; Kahn, P.; Vasiliu, M.: Dixon, D. A. Photodissociation and Theory to Investigate Uranium Oxide Cluster Cations. *J. Phys. Chem. A* **2020**, *124*, 10,1940-1953.

[71] Li, S.; Dixon, D. A. Molecular and Electronic Structures, Brönsted Basicities, and Lewis Acidities of Group VIB Transition Metal Oxide Clusters. *J. Phys. Chem. A* **2006**, *110*, 6231−6244.

[72] Kovács A. Relativistic Multireference Quantum Chemical Study of the Electronic Structure of Actinide Trioxide Molecules. *J Phys Chem A* **2017**, *121*, 2523–2530.

[73] Dau, P. D.; Vasiliu, M.; Wilson, R. E.; Dixon, D. A.; Gibson, J. K. Hydrolysis of Metal Dioxides Differentiates d-block from f-block Elements: Pa(V) as a 6d Transition Metal; Pr(V) as a 4f "Lanthanyl". *J. Phys. Chem. A* **2020**, *124*, 9272-9287.

TOC Graphic

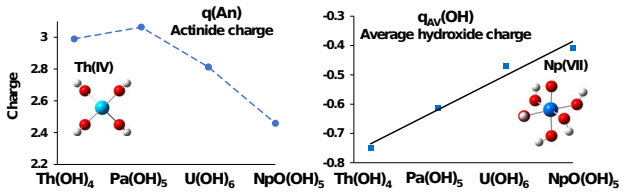

Covalency increases from Th(IV) to Np(VII)